

# Morphology of Highly Textured Poly(ethylene)/Poly(ethylene-propylene) (E/EP) Semicrystalline Diblock Copolymers

Peter Kofinas<sup>†</sup> and Robert E. Cohen\*<sup>‡</sup>

Department of Materials Science and Engineering and Department of Chemical Engineering, Massachusetts Institute of Technology, 77 Massachusetts Avenue, Cambridge, Massachusetts 02139

Received December 6, 1993; Revised Manuscript Received February 22, 1994\*

**ABSTRACT:** A series of semicrystalline diblock copolymers of poly(ethylene)/poly(ethylene-propylene) (E/EP) were subjected to high levels of plane strain compression using a channel die. Deformations were imposed both below and above the melting point of the E block. The crystallographic and morphological textures were examined using wide-angle X-ray diffraction pole figure analysis and two-dimensional small-angle X-ray scattering. The lattice unit cell orientation of the crystallized E chains with respect to the lamellar superstructure was determined, as well as the lamellar orientation relative to the specimen boundaries. When the diblocks are textured above the E block melting point at various compression ratios, the lamellae orient perpendicular to the plane of shear, while texturing below  $T_m$  causes the lamellae to orient parallel to the plane of shear. The orientation of the crystallized E chains was perpendicular to the lamellar normal, irrespective of the texturing temperature.

## 1. Introduction

In previous investigations in this laboratory,<sup>1-3</sup> the lattice unit cell orientation with respect to the lamellar microstructure was determined for semicrystalline diblock copolymers containing a crystallizable ethylene block. The orientation of the crystallized ethylene chains was found to be perpendicular to the lamellar normals. This unusual chain alignment was attributed to the influence of interface-dominated nucleation and topological constraints on growth when the ethylene block chains crystallize within the amorphous lamellar microdomains present in the heterogeneous melt phase of the block copolymers. Bates and co-workers<sup>4-6</sup> have studied the lamellar orientation of nearly symmetric amorphous poly(ethylene)/poly(ethylene-propylene) (E/EP) diblock copolymer samples, which were textured using large strain dynamic shear. Near the order-disorder transition (ODT) temperature, and at low shear frequencies, the lamellae arrange parallel to the plane of shear, while higher frequency processing leads to lamellae perpendicular to the plane of shear. At temperatures further below the ODT the parallel lamellar orientation is obtained at all shearing frequencies. These interesting and unexpected results prompted us to inquire into the possibility that semicrystalline block copolymer systems might also exhibit the perpendicular lamellar morphology under shear.

We have determined the lamellar orientation and chain organization upon crystallization for various processing histories near the ODT and below the crystallization temperature in a series of diblock copolymers having crystalline quasi-poly(ethylene) (E) blocks and amorphous poly(ethylene-propylene) (EP) blocks. Mechanical properties of E/EP diblocks and triblocks have been reported,<sup>7,8</sup> and some work has been done to characterize the morphology.<sup>8,9</sup> We have previously examined in considerable detail the gas transport properties of the E/EP polymers used in the present study.<sup>10</sup> Using the results presented below, we demonstrate that changes in the temperature of plane strain compression processing can be used to force

Table 1. Characterization of E/EP Specimens

sample	10 <sup>-3</sup> M		unit cell (Å)	
	E	EP	a	b
E/EP 30/70	30	70	7.56	4.98
E/EP 50/50	50	50	7.53	4.98
E/EP 60/40	60	40	7.52	4.96
E/EP 70/30	70	30	7.54	4.98
HDPE			7.43	4.95
E/EP 60/120	60	120		
E/EP 100/100	100	100		
E/EP 120/80	120	80		

the lamellae to orient either perpendicular or parallel to the plane of shear; the orientation of the crystallized E chains, however, always remains parallel to the plane of the lamellar superstructure irrespective of the processing temperature.

## 2. Experimental Section

The E/EP block copolymers were synthesized by hydrogenation of 1,4-poly(butadiene)/1,4-poly(isoprene) block copolymers. The butadiene block consists of 10% 1,2-, 35% *trans*-1,4-, and 55% *cis*-1,4-PB, while the isoprene block contains 93% *cis*-1,4- and 7% 3,4-PI. The catalytic hydrogenation procedure is described in detail elsewhere.<sup>11,12</sup> Hydrogenated PB thus resembles low-density polyethylene (E) and hydrogenated PI is essentially perfectly alternating ethylene propylene rubber (EP). The molecular weights of the E/EP diblocks are listed in Table 1. These values were determined from GPC measurements on the polydiene precursors (first block and diblock), from knowledge of reactor stoichiometry and conversion, and from a previous demonstration<sup>11</sup> that little or no degradation occurs during the hydrogenation reactions. The melting points of the crystallizable E blocks of the series of E/EP diblocks, were all between 99 and 103 °C, as determined by DSC.

A channel die, the description of which is given in detail elsewhere,<sup>13-16</sup> was used to subject the polymers to plane strain compression up to compression ratios of 11. Figure 1 shows a sketch of the channel die and defines the three principal directions, i.e., the lateral constraint direction (CD), the free (or flow) direction (FD), and the loading direction (LD). The channel die was maintained at a selected constant temperature during the compression flow, and the load was applied continuously until the desired compression ratios were achieved. The compressed specimens were quenched under load to room tempera-

<sup>†</sup> Department of Materials Science and Engineering.

<sup>‡</sup> Department of Chemical Engineering.

\* Abstract published in *Advance ACS Abstracts*, April 15, 1994.

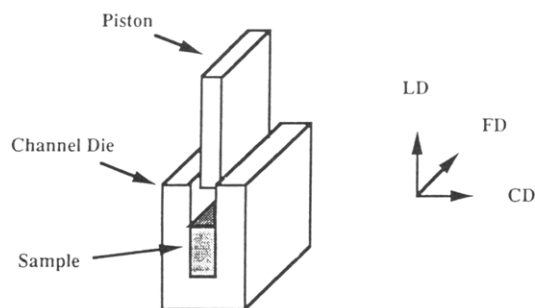


Figure 1. Channel die apparatus.

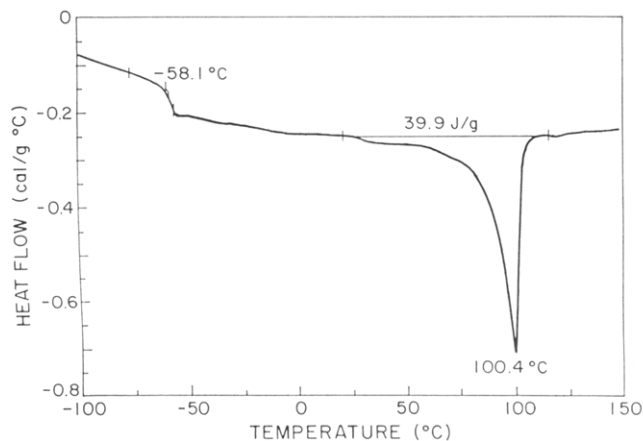


Figure 2. DSC scan for E/EP 30/70.

ture, followed by load release. The final compression ratio was determined from the reduction of the thickness of the samples.

The change in lamellar orientation due to deformation was studied by means of small-angle X-ray scattering (SAXS). The SAXS measurements were performed on a computer-controlled system consisting of a Nicolet two-dimensional position-sensitive detector associated with a Rigaku rotating-anode generator operating at 40 kV and 30 mA and providing Cu K $\alpha$  radiation. The primary beam was collimated by two Ni mirrors. In this way the X-ray beam could be effectively focused onto a beam stop with a very fine size without losing much intensity. The specimen to detector distance was 2.7 m, and the scattered beam path between the specimen and the detector was enclosed by an Al tube filled with helium gas in order to minimize the background scattering.

A separate Rigaku wide-angle X-ray diffractometer with a rotating-anode source was employed. The Cu K $\alpha$  radiation generated at 50 kV and 60 mA was filtered using a thin-film Ni filter to remove the K $\beta$  signal. A Rigaku pole figure attachment was controlled on-line, and X-ray diffraction data were collected by means of a Micro VAX computer running under DMAXB Rigaku-USA software. The slit system that was used allowed for collection of the diffracted beam with a divergence angle of less than 0.3°. Complete pole figures<sup>15</sup> were obtained for the projection of Euler angles of sample orientation:  $\beta$  from 0 to 360° with steps of 5°, and  $\alpha$  in the range 0–90° also in 5° steps. X-ray data from the transmission and reflection modes were connected at the angle  $\alpha = 50^\circ$ . The specimen orientation was such that the flow direction FD corresponds to the Euler angles of  $\alpha = 0^\circ, \beta = 90^\circ$  or  $\alpha = 0^\circ, \beta = 270^\circ$  (rotational symmetry), the constraint direction CD was at  $\alpha = 0^\circ, \beta = 0^\circ$  or  $\alpha = 0^\circ, \beta = 180^\circ$ , and the loading direction LD was at  $\alpha = 90^\circ$  (center of the stereographic projection).

### 3. Results

Figure 2 shows the DSC curve for the E/EP 30/70 polymer. The peak centered at 100.4 °C defines the nominal melting point of polyethylene in this sample. The large breadth of the melting curve indicates the presence of a wide distribution of crystal sizes and perfection. Crystallization occurs almost instantaneously as the

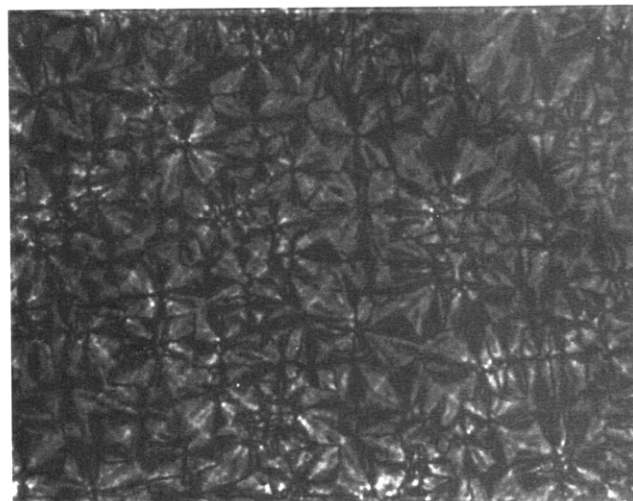
10  $\mu\text{m}$ 

Figure 3. Optical micrograph of E/EP 60/40 crystallized from the melt.

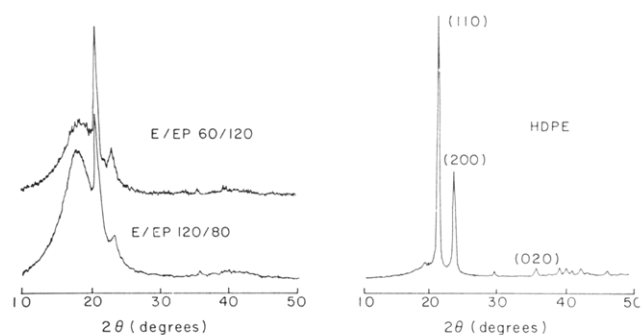


Figure 4. WAXS  $2\theta$  scans of E/EP diblocks.

polymers are cooled below their melting point; varying the thermal history has little observable effect on the degree of crystallinity. Using polarized light microscopy, we observed that all diblocks exhibit spherulitic morphology when crystallized from the melt, even in the sample containing as little as 30% polyethylene. These observations suggest that a lamellar morphology predominates over the entire composition range examined here. A representative micrograph of the spherulitic morphology of the E/EP polymers is shown in Figure 3.

The crystalline structure of undeformed spherulitic E/EP polymers is revealed in Figure 4 in the form of  $2\theta$  scans from the wide angle diffractometer. The diffraction peaks observed in the E/EP diblock copolymers correspond to the (110), (200), and (020) diffraction planes of the orthorhombic unit cell of polyethylene.<sup>17</sup> In addition to the diffraction planes, a broad amorphous halo centered around  $2\theta = 20^\circ$  is observed. The intensity of the amorphous halo increases as the amorphous block content in the diblock increases.

From the positions of the peaks in the  $2\theta$  scans of the E/EP samples (Figure 4) it is possible to calculate the  $a$ - and  $b$ -axis dimensions of the orthorhombic unit cell using the relationship<sup>17</sup>

$$\frac{1}{d_{hkl}^2} = \frac{h^2}{a^2} + \frac{k^2}{b^2} + \frac{l^2}{c^2} \quad (1)$$

where  $d_{hkl}$  is the spacing between crystallographic planes with Miller indices  $h$ ,  $k$ , and  $l$ , and  $a$ ,  $b$ , and  $c$  are the

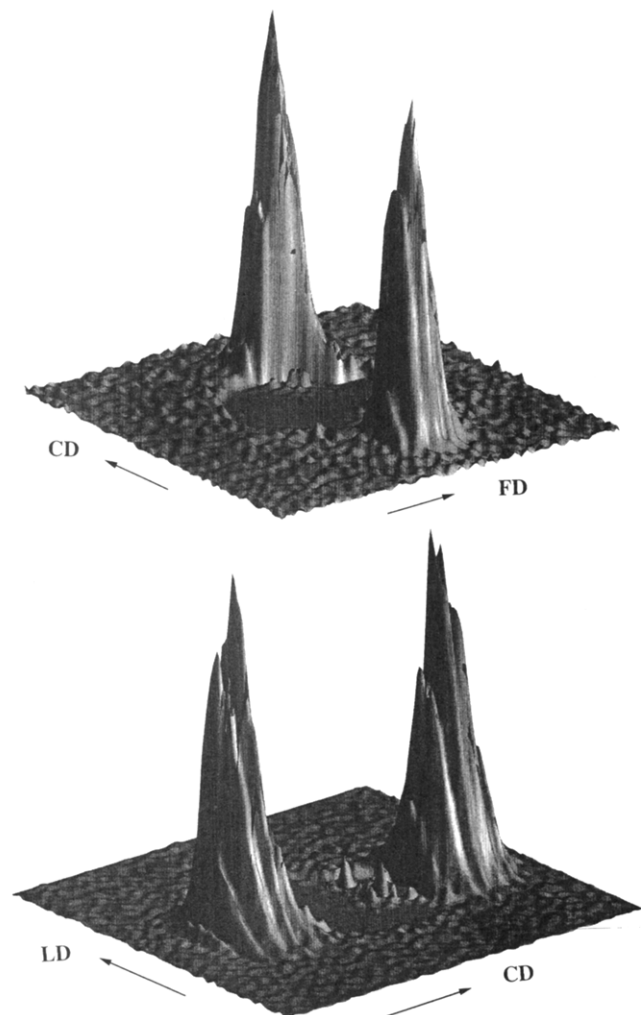


**Figure 5.** SAXS of E/EP 50/50 oriented above the E block melting point via plane strain compression: (a, top) X-ray beam in the loading direction; (b, bottom) X-ray beam in the flow direction.

dimensions of the unit cell. The values obtained are presented in Table 1. It is clear that the unit cell of E/EP is slightly larger than that of the HDPE homopolymer, which is in agreement with a previous investigation in this laboratory<sup>3</sup> on the unit cell dimensions in semicrystalline block copolymers containing an ethylene crystallizable block, and that there is no significant trend with amorphous content or copolymer molecular weight.

The 2D SAXS patterns of a representative E/EP specimen subjected to plane strain compression at 150 °C and then quenched to room temperature are shown in Figure 5. The channel die experiments were conducted at compression ratios of  $\lambda = 4$  to  $\lambda = 12$  with no observed change in the SAXS pattern. There is no significant scattering when the X-ray beam is parallel to the constraint direction. Spread-out spots on the 2D detector are observed when the sample is irradiated in the flow direction, in contrast to the sharp dots obtained when the X-ray beam is along the loading direction. The shape of the FD SAXS pattern is characteristic of the superposition pattern of lamellar stacks having different amounts of shear.<sup>18</sup> Figure 6 shows pole figures of the spatial density of normals to the (200), (020), and (110) planes for the same E/EP 50/50 specimen, which was compressed at 150 °C, i.e. well above the melting point of the E block. The pole figures represent views from the loading direction and are shown in the form of shade plots. A linear gray scale color map is used to represent intensity contours

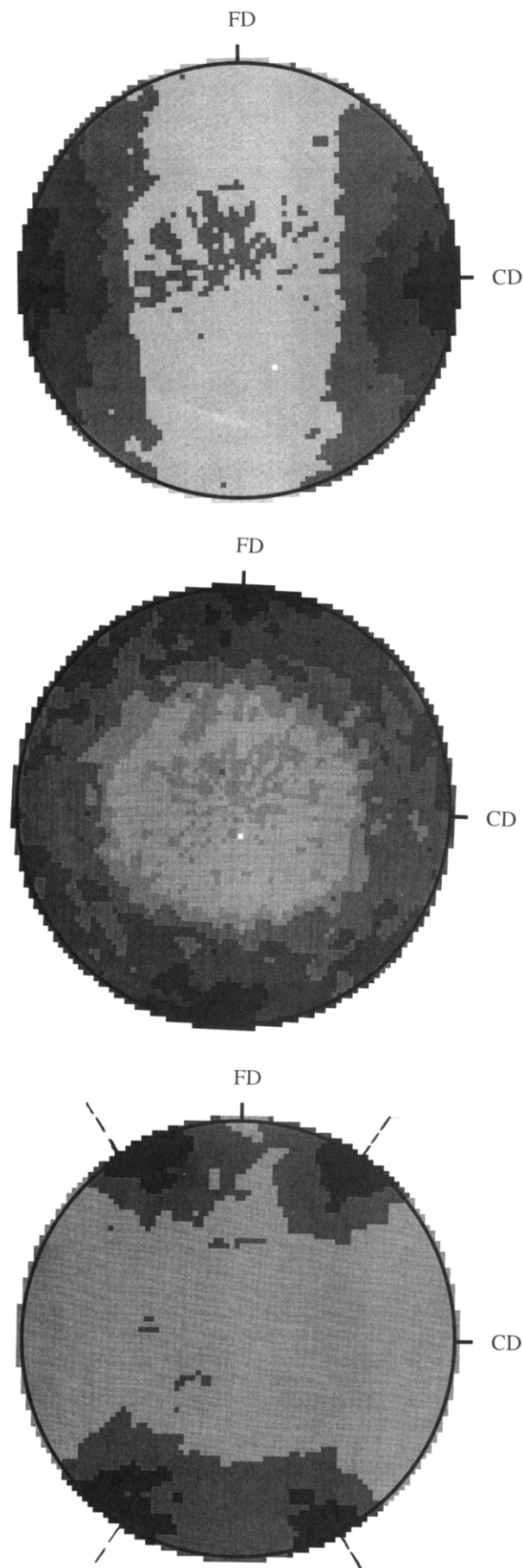


**Figure 6.** Pole figures of E/EP 50/50 oriented above the E block melting point via plane strain compression (top to bottom): (a) (200), (b) (020), (c) (110) planes. The dashed line represents the calculated position of the (110) poles.

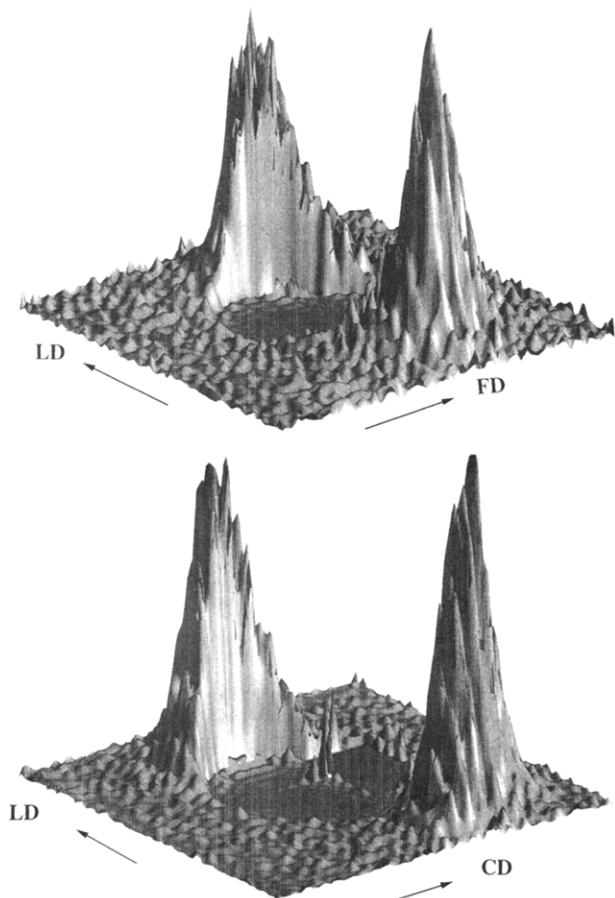


**Figure 7.** SAXS of E/EP 50/50 oriented below the E block melting point via plane strain compression: (a, top) X-ray beam in the constraint direction; (b, bottom) X-ray beam in the flow direction.

ranging from 5% to 90% of total intensity, with darker regions representing higher intensities of plane normals. The (200) and (020) poles are concentrated along the constraint and the flow direction, respectively, indicating that the chains are oriented in the loading direction.

All diblocks of total molecular weight 100 000 exhibited the same lamellar and chain orientation when textured at 150 °C except for the E/EP 70/30 specimen. The intensity of the scattering in the 2D SAXS pattern for this diblock was much lower than the other 100K specimens, indicating substantially weaker lamellar orientation, and the pole figure analysis revealed no information on the chain orientation, since no clustering of poles in any particular direction was observed. The E/EP diblocks having a large total molecular weight, namely the E/EP 60/120, 120/80, and 100/100 samples, showed no SAXS pattern, when deformed under the same conditions described above; this result arises because the lamellar long periods expected for these materials are beyond the range of detection in our SAXS equipment.

The E/EP 50/50 sample when textured at 80 °C (Figure 7) shows a set of SAXS patterns which are completely different from the results (Figure 5) obtained from the 150 °C channel die compression. The view from the loading direction reveals no scattering, arcs are observed along the loading direction upon irradiation parallel to the constraint direction (Figure 7a), and broad spots are obtained when the X-ray beam is parallel to the flow direction (Figure 7b). The SAXS patterns thus reveal that the morphology changes from lamellae oriented perpendicular to the plane of shear when the specimen is

deformed above the E block melting point, to lamellae oriented parallel to the shear plane for samples textured below the melt. The pole figures for the E/EP 50/50 specimen textured below the E block melting point (Figure 8) have the (200) poles in the loading direction and the (020) poles in the constraint direction, which implies that the *c*-axis of the polyethylene unit cell is oriented in the flow direction. Plane strain compression below the E melting point thus also results in a crystallized E chain orientation which is parallel to the plane of the lamellar superstructure.

The results for the lamellar orientation and the unit cell orientation within the crystallized lamellae in the textured E/EP 100K diblocks, as deduced from the pole figure and SAXS analysis, are summarized schematically in Figure 9.

#### 4. Discussion

The angle between the poles of two planes ( $h_1k_1l_1$ ) and ( $h_2k_2l_2$ ) for an orthorhombic unit cell is

$$\cos \phi = \frac{\frac{h_1h_2}{a^2} + \frac{k_1k_2}{b^2} + \frac{l_1l_2}{c^2}}{\sqrt{\left(\frac{h_1^2}{a^2} + \frac{k_1^2}{b^2} + \frac{l_1^2}{c^2}\right)\left(\frac{h_2^2}{a^2} + \frac{k_2^2}{b^2} + \frac{l_2^2}{c^2}\right)}} \quad (2)$$

All the poles of the crystallographic reflections presented in Figures 6 and 8 belong to the form  $\langle hk0 \rangle$  and thus lie on the same plane. Using eq 2 and the values for the E/EP unit cell from Table 1, the location of the (110) pole lies in the CD–FD plane at an angle  $\phi = 56.6^\circ$  with respect to the (200) pole. The calculated angle  $\phi$  between the (200) and (110) poles is in excellent agreement with the location of the (110) pole, as shown in Figure 7c, thus confirming the proposed chain orientation and the assumption of the orthorhombic unit cell. For the E/EP 50/50 specimen textured at 80 °C, the same angle  $\phi$  between the (200) and (110) poles is found in the LD–CD plane. In all of our specimens the (200) and (020) pole figures alone are sufficient to determine the unit cell orientation. The (110) pole figures are presented, however, as additional supporting evidence to confirm the proposed unit cell orientations.

The average intensities of the SAXS patterns of the channel die samples at 150 °C were calculated for rectangular slices along the lamellar normal, i.e. the CD direction, to determine the lamellar long periods  $D_{LD}$  and  $D_{FD}$ , and a representative plot is shown in Figure 10 as a plot of intensity  $I(Q)$  versus scattering vector magnitude  $Q$  ( $Q = (4\pi/\lambda) \sin \theta$  and the scattering angle is  $2\theta$ ). Because of the symmetry of the SAXS pattern there are always two peaks at  $+Q$  and  $-Q$ . The absence of data points around  $Q = 0$  is due to the beamstop. The data are shown with solid points together with a solid line representing a cubic smoothing spline fit. Table 2 compares the lamellar long periods  $D_{LD}$  and  $D_{FD}$  calculated for each specimen from the integrated SAXS spectra of Figure 10. The FD spectra show somewhat shorter average *D* spacings than the ones calculated from the LD SAXS spectra, but the difference is within the 10% error range in the calculation of the lamellar long periods.

The behavior of the E/EP diblocks, when textured in the melt, can be rationalized from an examination of the position of the diblocks with respect to Leibler's phase diagram<sup>19</sup> and using the results of previous studies on wholly amorphous diblock copolymers.<sup>6</sup> Diblock copolymers contain two long sequences with  $N_A$  and  $N_B$  units of

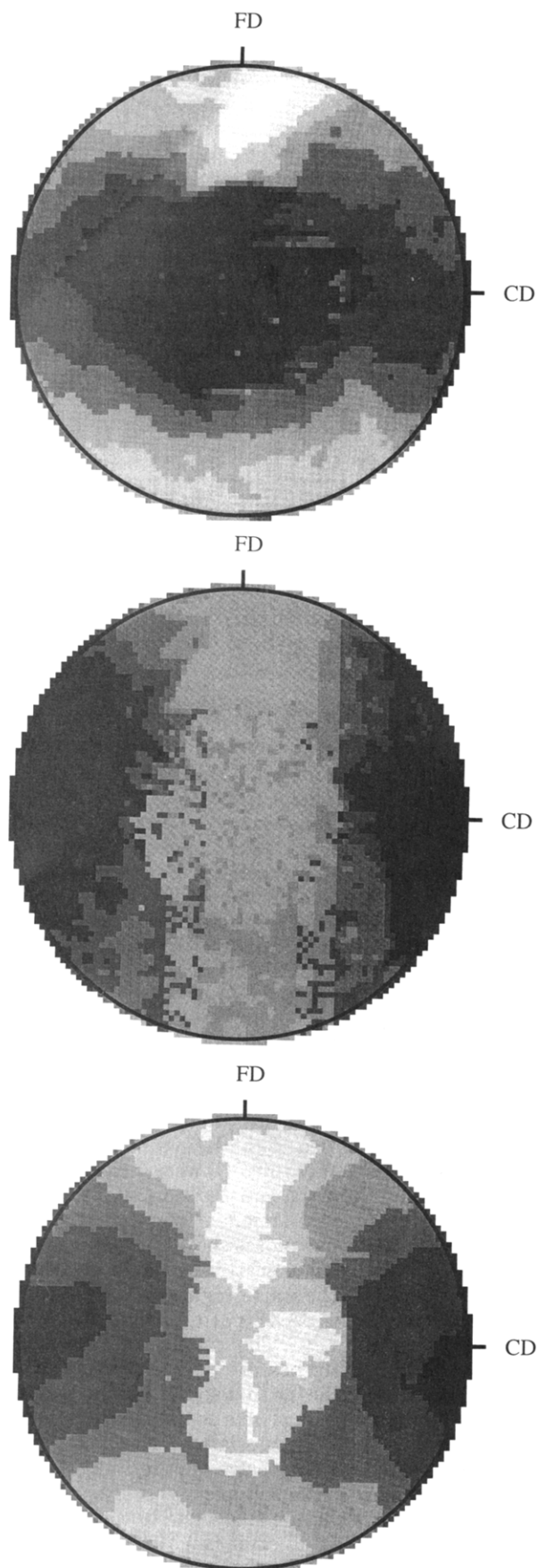


**Figure 8.** Pole figures of the E/EP 50/50 diblock oriented below the E block melting point via plane strain compression (top to bottom): (a) (200), (b) (020), (c) (110) planes.

chemically distinct segments. At sufficiently high temperatures (or low total degree of polymerization  $N_T = N_A$

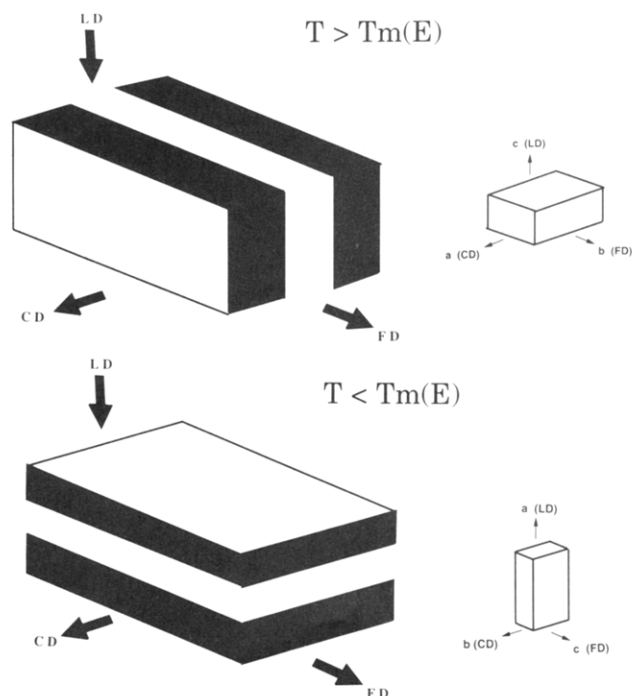


**Figure 9.** Sketch of lamellar and unit cell orientation in E/EP specimens processed above (a, top) and below (b, bottom) the E block melting point. The insert shows the orientation of the orthorhombic PE unit cell.

+  $N_B$ ) the melt is disordered or homogeneous, while at low temperatures (or high  $N_T$ ) various ordered structures<sup>19</sup> (lamellar, OBDD, hexagonal, cubic) are observed. Equilibrium phase behavior was expressed by Leibler in terms of the polymer composition  $f$  and the reduced parameter  $\chi N_T$ , where  $\chi$  represents the Flory-Huggins segment-segment interaction parameter.  $\chi N_T$  for each of our diblocks was calculated using  $\chi$  values reported by Bates et al.;<sup>20</sup> the results are plotted versus the E fraction in the copolymer in the format of Leibler's phase diagram at 100 and 150 °C in Figure 11. The highest molecular weight diblocks for this study (upper row of solid points on the phase diagram) are clearly above the order-disorder boundary for both of the selected temperatures, thus indicating that at equilibrium they form heterogeneous melts; the 100K diblocks, however, are very close to the order-disorder transition (ODT).

The results shown in Figure 11 show that all of our 100K diblocks are being processed in the 150 °C channel die experiments exactly in the regime near the ODT in which fluctuations<sup>6</sup> dominate the lamellar structure of the melt. In this regime of the morphological phase diagram, the diblock copolymers have already been shown to respond to shear deformation by organizing their lamellar structure perpendicular to the plane of shear.<sup>4</sup> This peculiar orientation was attributed<sup>6</sup> to the disordering ("melting") of the lamellae with immediate regrowth. The thermodynamic barrier to disordering was overcome only near the ODT; thus production of perpendicular lamellae only occurs near the ODT.<sup>6</sup> We find the same behavior here for the case of plane strain compression of our 100K specimens at 150 °C. We therefore conclude that our E/EP diblocks form ordered heterogeneous melts under the shear field imposed from the channel die, when deformed at 150 °C above the E block melting point. As the sample is cooled under load, the perpendicular lamellar phase is subsequently "frozen-in" at the onset of crystallization. The crystallization therefore is required to occur in the presence of this preexisting lamellar morphology, a situ-

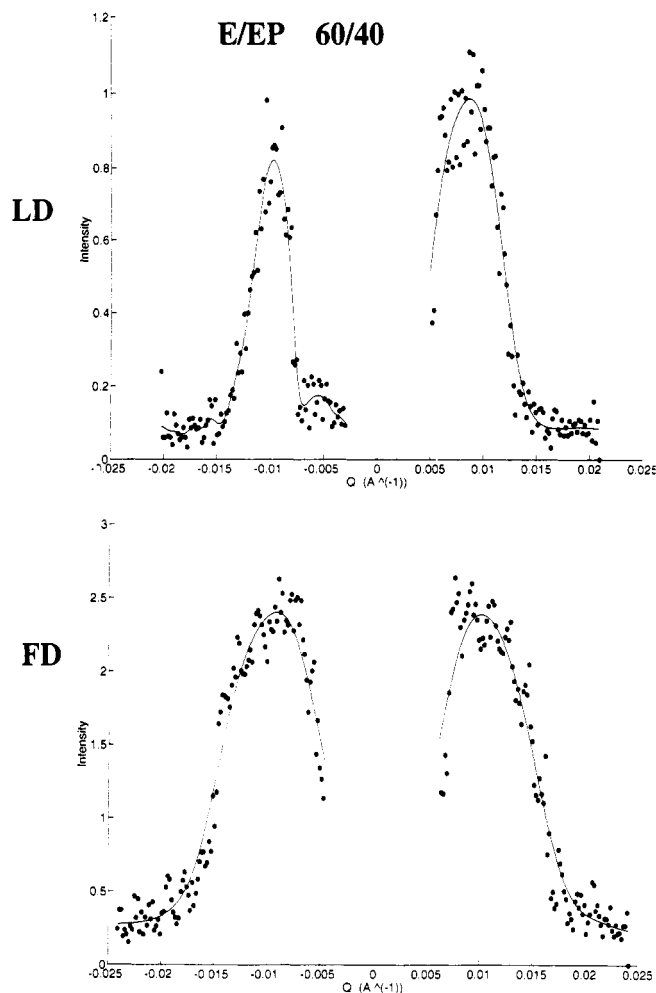


**Figure 10.** Averaged SAXS spectra for the uniaxially compressed E/EP 60/40 diblock above the E block melting point. LD: X-ray beam in the loading direction. FD: X-ray beam in the flow direction.

**Table 2. Lamellar Long Periods for Channel Die Samples at  $T = 150\text{ }^{\circ}\text{C}$**

sample	$D_{LD}$ (Å)	$D_{(FD)}$ (Å)
E/EP 30/70	618	598
E/EP 50/50	601	557
E/EP 60/40	665	604
E/EP 70/30	556	551

ation which has already been shown<sup>1,2</sup> clearly to lead to the type of unit cell orientation (chains perpendicular to the lamellar normals) shown in Figure 9.

The deformation mechanisms involved in producing the channel die samples below the E block melting point, which result in a "parallel lamellar" morphology, are mostly crystallographic in nature,<sup>15</sup> similar to those found in the sub- $T_m$  plastic deformation of many polycrystalline materials. The crystallized E chains are once again always perpendicular to the normals of the lamellar superstructure, but in this case the crystallographic texture is deformation-induced, unlike the interface-dominated crystallization of confined chains mentioned above.

Although the long period spacings of the higher molecular weight samples precluded direct observation of lamellar orientation for these materials, we still may conclude that the channel die processing did not produce any oriented lamellar morphology upon plane strain compression at  $150\text{ }^{\circ}\text{C}$  of the E/EP 60/120, 100/100, and 120/80 diblocks. This statement is based on the absence of any orientation in the pole figures of these samples. Thus, for the case of semicrystalline block copolymers,

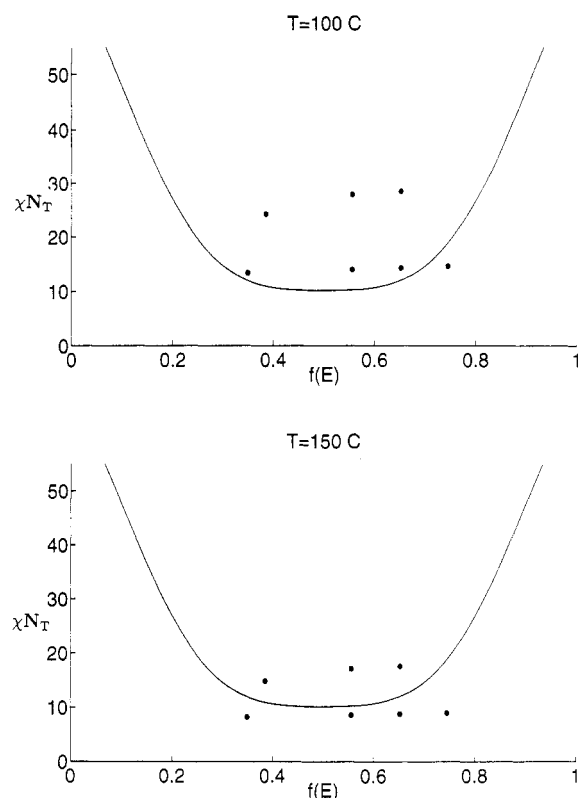


**Figure 11.** Position of our copolymers relative to the order-disorder transition curve of Leibler's phase diagram: (a, top)  $T = 100\text{ }^{\circ}\text{C}$ ; (b, bottom)  $T = 150\text{ }^{\circ}\text{C}$ .

the determination of the unit cell texture via the WAXS pole figure analysis provides an added probe for determining what has happened to the material processed in the melt.

## 5. Summary

We have shown by SAXS that two distinct lamellar orientations can be produced when a series of semicrystalline E/EP diblock copolymers of varying E block content and 100 000 total molecular weight are subjected to high levels of plane strain compression. When the diblocks are deformed above the E block melting point at various compression ratios, the lamellae orient perpendicular to the plane of shear, while texturing below the melt causes the lamellae to orient parallel to the plane of shear. The morphology produced above the melting point was attributed to the proximity of the order-disorder transition to the processing temperature. Although several examples of the unexpected perpendicular orientation have been reported for amorphous diblock copolymers, to the best of our knowledge this is the first experimental documentation of perpendicular orientation in sheared semicrystalline block copolymer lamellar phases. The semicrystalline diblocks exhibit the perpendicular lamellar orientation for a much broader composition range than any amorphous diblock system reported to date. Furthermore, the semicrystalline systems offer the advantage that the crystallographic texture, which is eventually locked into the materials when cooled below  $T_m$ , provides an independent set of clues regarding the orientation of the lamellae at the point when crystallization takes place. Conversely, the deformation mechanisms at  $T < T_m$ , which lead to the series lamellar morphology, are crystallographic in nature. WAXS pole figure analysis has revealed that the orientation of the crystallized E chains is perpendicular to the lamellar normal, irrespective of the deformation temperature. When the processing is carried out above

$T_m$ , the heterogeneous melt orients perpendicular to the shear planes, and then upon cooling, the E block chains crystallize within the amorphous lamellar microdomains, a process which has been shown to generate a crystallographic texture with chains perpendicular to the lamellar normals.<sup>1,2</sup>

The unusual shear-induced perpendicular lamellar morphology may have some potential advantages; for example, it provides a "parallel" material from the perspective of transport through a film. We have made use of this structure in an earlier study<sup>10</sup> of gas transport in these same semicrystalline block copolymers. The structure in which the alternating amorphous and semicrystalline lamellae are oriented normal to the film surfaces enables the membrane designer to enjoy the structural and thermal stability offered by the semicrystalline regions without having them interfere with the gas flux through the amorphous lamellae.

In our work to date we have examined only diblock copolymer structures. Ongoing research includes studies of tri- and tetrablock copolymers of E/EP covering a wide range of composition and molecular weight.

**Acknowledgment.** This research has been supported by the Office of Naval Research and the Goodyear Tire and Rubber Co.

#### References and Notes

(1) Douzinas, K. C.; Cohen, R. E. *Macromolecules* **1992**, *25*, 5030.

- (2) Cohen, R. E.; Bellare, A.; Drzewinski, M. A. *Macromolecules*, in press.
- (3) Douzinas, K. C.; Cohen, R. E.; Halasa, A. F. *Macromolecules* **1991**, *24*, 4457.
- (4) Almdal, K.; Koppi, K. A.; Bates, F. S. *Macromolecules* **1992**, *25*, 1743.
- (5) Koppi, K. A.; Tirrell, M.; Bates, F. S. *Phys. Rev. Lett.* **1993**, *70* (10), 1449.
- (6) Koppi, K. A.; Tirrell, M.; Bates, F. S.; Almdal, K.; Colby, R. H. *J. Phys. II* **1993**, *2* (11), 1941.
- (7) Mohajer, Y.; Wilkes, G. L.; Wang, J. E.; McGrath, J. E. *Polymer* **1982**, *23*, 1523.
- (8) Seguela, R.; Prud'homme, J. *Polymer* **1989**, *30*, 1446.
- (9) Rangarajan, P.; Register, R. A.; Fetters, L. J. Blends of Amorphous and Crystalline Polymers Symposium; ACS National Meeting, August 1992, Washington, DC, Division of Polymer Chemistry; *Polym. Prep. (Am. Chem. Soc., Div. Polym. Chem.)* **1992**, *33* (2); *Macromolecules*, in press.
- (10) Kofinas, P.; Cohen, R. E.; Halasa, A. F. *Polymer*, in press.
- (11) Halasa, A. F. U.S. Patent 3 872 072.
- (12) Cohen, R. E.; Cheng, P.-L.; Douzinas, K.; Kofinas, P.; Berney, C. V. *Macromolecules* **1990**, *23*, 324.
- (13) Lin, L.; Argon, A. S. *Macromolecules* **1992**, *25*, 4011.
- (14) Song, H. H.; Argon, A. S.; Cohen, R. E. *Macromolecules* **1990**, *23*, 870.
- (15) Galeski, A.; Argon, A. S.; Cohen, R. E. *Macromolecules* **1992**, *25*, 5705.
- (16) Gray, R. W.; Young, R. J. *J. Mater. Sci.* **1974**, *9*, 521.
- (17) Spruiell, J. E.; Clark, E. S. *Methods of Experimental Physics*; Academic Press: New York, 1980; Vol. 16B, Chapter 6.
- (18) Song, H. H.; Argon, A. S.; Cohen, R. E. *Macromolecules* **1990**, *23*, 870.
- (19) Leibler, L. *Macromolecules* **1980**, *13*, 1602.
- (20) Bates, F. S.; Schultz, M. F.; Rosedale, J. H. *Macromolecules* **1992**, *25*, 5547.